Simultaneous observations of field-aligned beams and gyrating ions in the terrestrial foreshock

K. Meziane,[1] M. Wilber,[2] C. Mazelle,[3] D. LeQuéau,[4] H. Kucharek,[5] E. A. Lucek,[6] H. Rème,[3] A. M. Hamza,[1] J. A. Sauvaud,[3] J. M. Bosqued,[3] I. Dandouras,[3] G. K. Parks,[2] M. McCarthy,[7] B. Klecker,[8] A. Korth,[9] M. B. Bavassano-Cattaneo,[10] and R. N. Lundin[11]

Received 26 December 2003; revised 16 March 2004; accepted 7 April 2004; published 27 May 2004.

[1] We examine an energetic (2–30 keV) upstream ion event presenting a clear double-peak spectrum observed ~1 R_E upstream from the bow shock. The lower-energy ($E \sim 3.5$ keV) peak is associated with an ion beam propagating along the magnetic field direction, while the higher-energy ($E \sim 13$ keV) peak is associated with gyrating ions having pitch angles ~30°. The latter population progressively extends to lower energies over the span of the event. During times when the field-aligned beams were observed, the interplanetary magnetic field was remarkably steady, while the appearance of the 30° pitch angle gyrating ions was accompanied by the onset of large-amplitude ultralow frequency fluctuations of the magnetic field. Our analysis indicates that the gyrating ions had guiding centers on field lines downstream of the field-aligned component but that both populations could be sampled simultaneously because of the orbits of the former. We find that the downstream limit of the field-aligned beams is populated with protons having a speed 1.68 times the solar wind velocity, which is inconsistent with any known shock-related emission mechanisms. This boundary makes an angle of 77° with respect to the Sun-Earth line in agreement with theoretical predictions. Just downstream of this rapid transition, gyrating ions having a flow speed of 1.52 times the solar wind speed are observed in association with ULF waves. Like the field-aligned beams, the gyrating ions reported here have streaming speeds inconsistent with any known shock emission mechanisms. While the simultaneous observation of field-aligned and gyrating components is possible because of the large gyration orbits of the latter, the observational sequence is consistent with a very sharp ($\lesssim$1 gyroradius) boundary separating the guiding centers of each. Explicit observations of such a sharp demarcation between these populations have not been reported before, and they place a significant constraint on the production mechanisms of the two populations. Our interpretation of these observations provides a refinement of the usual framework for foreshock morphology. *INDEX TERMS:* 2116 Interplanetary Physics: Energetic particles, planetary; 2164 Interplanetary Physics: Solar wind plasma; 2134 Interplanetary Physics: Interplanetary magnetic fields; 2154 Interplanetary Physics: Planetary bow shocks; 7851 Space Plasma Physics: Shock waves; *KEYWORDS:* foreshock boundary, ultralow frequency waves, bow shock, field-aligned beam, magnetic moment, shock emission mechanism

Citation: Meziane, K., et al. (2004), Simultaneous observations of field-aligned beams and gyrating ions in the terrestrial foreshock, *J. Geophys. Res.*, *109*, A05107, doi:10.1029/2003JA010374.

1. Introduction

[2] It is now well known that regions upstream of the Earth's bow shock that are connected via magnetic field lines are populated by several types of ion populations [e.g., *Lin et al.*, 1974; *Gosling et al.*, 1978; *Bonifazi and Moreno*, 1981a; *Paschmann et al.*, 1981; *Gurgiolo et al.*, 1981]. The differing ion types statistically have a dependence on the shock geometry, which is determined by the angle θ_{Bn} that

[1]Department of Physics, University of New Brunswick, Fredericton, New Brunswick, Canada.
[2]Space Sciences Laboratory, University of California, Berkeley, California, USA.
[3]Centre d'Etude Spatiale des Rayonnements, Toulouse, France.
[4]Observatoire Midi-Pyrénées, Toulouse, France.
[5]Department of Physics and Institute for the Study of Earth, Oceans and Space, University of New Hampshire, Durham, New Hampshire, USA.
[6]Blackett Laboratory, Imperial College London, London, UK.
[7]Department of Earth and Space Sciences, University of Washington, Seattle, Washington, USA.
[8]Max-Planck Institut für Extraterrestrische Physik, Garching, Germany.
[9]Max-Planck Institut für Aeronomie, Katlenburg-Lindau, Germany.
[10]Istituto di Fisica dello Spazio Interplanetario, CNR, Rome, Italy.
[11]Swedish Institute for Space Physics, Kiruna, Sweden.

0148-0227/04/2003JA010374$09.00

the magnetic field makes with the local shock normal. Ion beams of several keV collimated along interplanetary field lines are usually observed upstream from the quasi-perpendicular shock. Intermediate ion distributions, having a broad spread in velocity space centered on the magnetic field, are seen just downstream of the field-aligned beam region. Finally, diffuse ion populations, distributed in a shell of nearly constant radius about an average velocity, are found upstream of the quasi-parallel shock [*Gosling et al.*, 1978; *Bonifazi and Moreno*, 1981a; *Paschmann et al.*, 1981]. Generally, the bulk velocities of upstream ions decrease with θ_{Bn} [*Bonifazi and Moreno*, 1981b].

[3] Using high-time resolution measurements, *Fuselier et al.* [1986] showed that many ion distributions previously thought to have the intermediate form are in fact gyrating ion beams. The later are characterized by peaks in phase space density (PSD) at nonzero pitch angles. The authors noted that the gyrating ions were associated with quasi-monochromatic ultralow frequency (ULF) waves.

[4] Upstream ion populations have been extensively studied [*Paschmann et al.*, 1981; *Bonifazi and Moreno*, 1981b; *Gurgiolo et al.*, 1983], and hypotheses have been put forward to explain their origin. It is believed that field-aligned beams observed in the quasi-perpendicular regions are produced by adiabatic reflection of a portion of the solar wind [*Paschmann et al.*, 1980] or by leakage from the magnetosheath [*Thomsen et al.*, 1983a]. A recent study by Wilber et al. (Cluster observations of shock production efficiencies for field-aligned beams, submitted to *Annales Geophysicae*, 2003, hereinafter referred to as Wilber et al., submitted manuscript, 2003) suggests that the observed characteristics are in partial conflict and partial agreement with both the adiabatic reflection model of *Sonnerup* [1969] and *Paschmann et al.* [1980] and with the magnetosheath escape model of *Tanaka et al.* [1983]. The field-aligned beams propagating through the ambient solar wind plasma generate electromagnetic waves as the result of streaming instabilities [*Gary et al.*, 1981]. These waves are convected downstream and may trap ions during the early wave growth process, leading to gyrating beams [*Hoshino and Terasawa*, 1985; *Meziane et al.*, 2001; *Mazelle et al.*, 2000, 2003]. Simulations and analytic studies indicate that as wave growth saturates, ions can be pitch angle scattered, resulting in intermediate distributions [e.g., *Winske and Leroy*, 1984; *Lee and Skadron*, 1985]. In both cases the original beam is destroyed. Gyrating ions may also be produced at the shock itself by the specular reflection of solar wind ions in quasi-parallel regions [*Gosling et al.*, 1982; *Meziane et al.*, 2004]. Another possible source for intermediate distributions is leakage across the shock from the magnetosheath [*Edmiston et al.*, 1982], but this has not been confirmed observationally.

[5] The phenomenology of each population, including the spatial distribution in the foreshock, has been extensively studied by *Bonifazi and Moreno* [1981a]. Velocity filtering of particles streaming away from the bow shock leads to a natural categorization of these populations according to the ratio $P_{gc} = V_{gc}/V_{sw}$, where V_{gc} is their guiding center speed (in the spacecraft frame of reference) and V_{sw} is the solar wind speed. Using the Solar Wind Experiment on board the ISEE 2 spacecraft, *Bonifazi and Moreno* [1981a] reported average values of $\langle P_{gc} \rangle = 2$ for the field-aligned beam, $\langle P_{gc} \rangle = 1.75$ for the intermediate ions, and $\langle P_{gc} \rangle = 1.18$ for diffuse populations. The spreads in these ratios were $\sim$0.5 and may reflect the fact that the statistical sample included a wide range of cone angles θ_{BV}. To date, P_{gc} values for gyrating ions have not been systematically studied. The field-aligned beams are found in a thin layer (spanning $\sim$0.4 R_E at ISEE distances) downstream from the $P_{gc} = 2$ boundary, followed farther downstream by a $\sim$3.5 R_E-wide layer of intermediate ions. Gyrating ions are located within this second layer, or possibly within a distinct thin layer between the field-aligned beams and the intermediate populations. We stress, however, that these results should be considered statistical in nature, and an important classification according to the cone angle θ_{BV} remains to be conducted.

[6] Recently, *Möbius et al.* [2001] reported simultaneous observations of field-aligned beams and gyrating ion distributions in the ramp of the bow shock. The gyrating ions were consistent with specular reflection of a large fraction of the solar wind stream, and the authors interpreted the emerging beams as a portion of the ring distribution that had been strongly pitch angle scattered immediately after reflection, as originally suggested by *Giacolone et al.* [1994]. The subject of the present study is different, as it considers the simultaneous observation of two populations that have different energies and are well upstream ($\sim$1 R_E) from the bow shock.

[7] Intermediate ions and gyrating beams are observed in association with large-amplitude ($\partial B/B \sim 1$) ULF waves. Gyrating ions are seen in the presence of quasi-monochromatic waves, while intermediate distributions are often observed when irregular waveforms are seen [*Fuselier et al.*, 1986]. For several cases studied, *Meziane et al.* [2001] showed that the waves are right-handed and propagate nearly along the ambient magnetic field. These are observed downstream from, and are likely produced by, field-aligned ions that interact with the solar wind beam through a beam plasma instability [*Gary et al.*, 1981; *Meziane et al.*, 2001].

[8] Field-aligned ion beams and gyrating distributions have not previously been observed simultaneously, suggesting the existence of a spatial boundary between the two populations. Moreover, statistical studies of ULF waves showed that for a given cone angle, there is a boundary separating regions of strong fluctuations from those with no fluctuations present [*Greenstadt and Baum*, 1986]. Using observations from ISEE 1's unidirectional Berkeley-Toulouse particle detector, *Meziane and d'Uston* [1998] showed that flux enhancement onsets for a given cone angle range are spatially organized. Because the field of view of this detector pointed in the $-z_{GSE}$ direction, little information was available on the nature of the distribution functions. However, for most field orientations the presence of particles along this axis would require particles offset from the field direction. These flux onsets could therefore be expected to statistically represent the boundary demarking intermediate and possibly gyrating ions. Despite instrumental limitations, this boundary was found to coincide with the ULF foreshock boundary reported by *Greenstadt and Baum* [1986] when the cone angle was in the range 40°–50°. In another study involving ULF wave morphology, *Le and Russell* [1992] showed the existence of a ULF boundary as defined above but

located upstream of the one found by *Greenstadt and Baum* [1986]. The latter study used larger statistics than applied in the former but was based on observations near the shock.

[9] In the present study, we report for the first time the observation of a gyrating ion distribution located almost at the lower spatial limit of the field-aligned ion beam region. We discuss the event in the context of the ULF/intermediate foreshock boundary presented above. The location and scale thickness of this boundary could be a test of models involving wave-particle interactions occurring in the foreshock region and of shock emission mechanisms.

[10] We briefly describe the Cluster Ion Spectrometer (CIS) experiment in section 2. The observations are presented in section 3 and are followed by an analysis of the geometry in section 4. A possible source of ions propagating along the boundary is then discussed in section 5.

2. Experiment

[11] The particle data used in this study are from the CIS experiment, which includes a hot ion analyzer (HIA) that measures ions with no species discrimination using a top hat electrostatic analyzer (ESA), and a mass spectrometer (the Composition Distribution Function experiment (CODIF)), which combines an ESA with a time-of-flight back end to measure the major species H^+, He^+, He^{++}, and O^+. These sensors span energy ranges of 0.005–38 keV q^{-1} and 0.01–38 keV q^{-1}, respectively. Each has two sides with differing geometry factors. For HIA these are 5×10^{-3} and 5×10^{-4} cm^2 sr, and for CODIF they are 2×10^{-2} and 2×10^{-4} cm^2 sr. The low-geometry factor sides are used to measure the high-flux solar wind beam. When the solar wind operational modes are in effect, the energy sweeps are truncated on the high-geometry factor side as the sensor aperture rotates into the sunward looking direction. This prevents saturation and accounts for why the solar wind beam is largely absent from these data products. Both instruments accumulate full three-dimensional (3-D) distributions within one 4-s satellite spin period, although during typical modes two or three spins are averaged prior to telemetry. In high angular resolution or high-energy resolution modes, CODIF requires an extra spin to process the data for telemetry, reducing the cadence accordingly. These detectors have an angular resolution of $22.5° \times 22.5°$. In normal telemetry mode, one distribution is transmitted every two spins (or three spins depending on the time period), whereas in burst mode an HIA distribution is transmitted every spin. A detailed description of the Cluster/CIS experiment can be found in work by *Rème et al.* [2001]. With the above instrumental characteristics both the solar wind plasma as well as the energetic particles are detected.

[12] Our study also uses magnetic field data which come from the fluxgate magnetometer (FGM) installed on board the Cluster spacecraft [*Balogh et al.*, 2001]. We have used spin resolution magnetic field components to investigate the association of low-frequency waves with the backstreaming ions. The data for this study were obtained during polar cusp crossing orbits, which typically graze the shock surface and rarely penetrate far into the upstream. We use observations from spacecrafts 1 and 3; during the time of interest these spacecraft were separated by ~500 km.

3. Observations and Data Analysis

[13] Figure 1 shows observations recorded on 3 February 2001 while Cluster spacecraft 1 (SC 1) was at (15.60, 5.38, −4.08) R_E (GSE). The first panel shows the proton energy spectrogram measured by CODIF (high-G mode) at 12 s resolution and because of the energy sweep cutoff in sunward look directions, excludes the solar wind beam. During the 2108:00–2109:17 UT time interval the spectra are narrowly peaked from 1–8 keV (hereafter ~3 keV), with these fluxes corresponding to particle beams streaming away from the bow shock. The solar wind component is not observed while the detector is operating in its solar wind mode. At 2109:21 UT, 10–30 keV (hereafter ~17 keV) protons appear for ~2 min. During this span the lower energy limit to the ~17 keV component decreases until the two components have merged into a broader peak.

[14] Figure 1 (second, third, and fourth panels) shows plasma densities and velocities from HIA's low-geometry factor side every spin period (4 s). These remain very steady at ~4.2 cm^{-3} until 2111:15, after which time the density increases by 20% for ~1.5 min. This is followed by a reduction in average density to ~3.5 cm^{-3}, with large-amplitude, quasiperiodic oscillations of ~40 s duration that extend well beyond the interval shown. At about the same time the velocities begin to show small perturbations. The fifth panel presents magnetic field vectors from FGM, also at 4 s resolution. The field is very steady until 2111:15, after which time it undergoes large $\delta B/B$, 40 s modulations. The field magnitude (top trace) indicates that there is some compressional component to the observed waves.

[15] The merging of the ~17 keV component with the few keV component follows the modest increase in density (and dynamic pressure), but time delays for the pressure variation to reach the shock and for backstreaming particles to then return to Cluster probably rule out shock compression as an explanation for the merging of the two particle components. The broader particle spectrum appearing after 2112:01 UT coincides with the density oscillations and the magnetic field modulations seen during the second half of the interval plotted.

[16] Figure 2 shows 12-s (three spin) snapshots of proton spectra measured at different time intervals. We note that during this period the average proton cyclotron period is ~15 s. The energy spectrum taken at 2109:05–2109:17 UT (dashed curve) indicates the presence of a single component with an energy cutoff at ~8 keV. Later on, particularly at 2110:57–2111:09 UT, the spectra indicate the presence of a secondary beam in the energy range E = 10–30 keV. The secondary beam is still present at 2111:29–2111:41 UT, although its peak has shifted down to ~10 keV. These first three curves show a gradual broadening of the low-energy peak, with the maximum flux shifting slightly toward lower energies. By 2112:01–2112:13 UT the spectrum shows no clear corresponding ~10 keV peak and appears as a single, warmer population.

[17] Figure 3 shows 3-D measurements of the particle distributions from SC 1 obtained between 2109:05 and 2112:45 UT. The Hammer-Aitoff projection [*Meziane et*

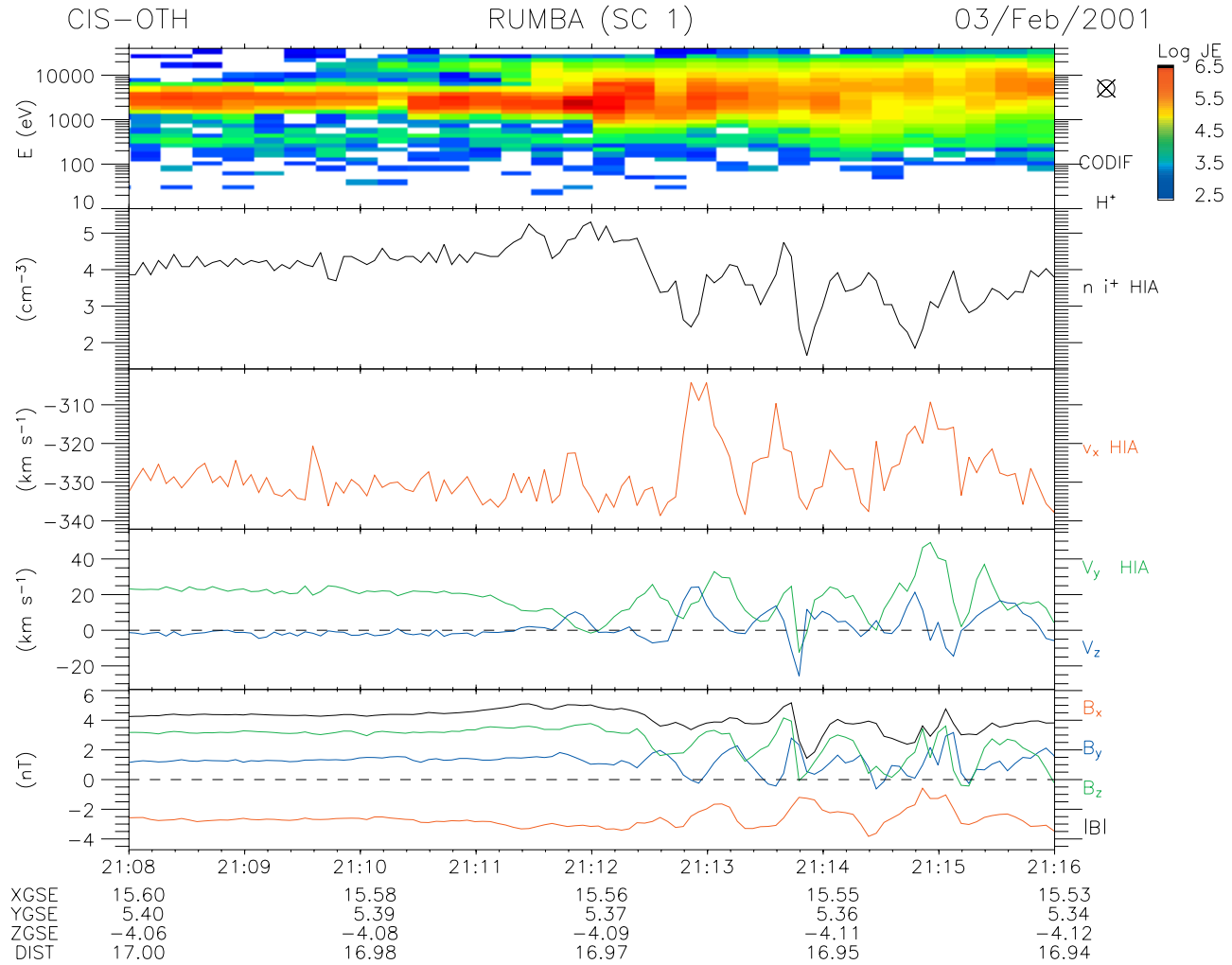

Figure 1. Proton spectrogram obtained from Cluster 1 CODIF instrument (first panel), solar wind density (second panel) and solar wind velocity (third and fourth panels) from HIA instrument, and the three IMF components in the GSE frame of reference (fifth panel).

al., 2001; *Mailing*, 1992] is used to display 4π sr projections of the distributions for the energy channels 17.74, 14.08, 3.83, 3.15, and 2.62 keV. With upstream particles streaming primarily opposite to the magnetic field, these 2-D slices are centered on the antifield-aligned direction (indicated by a diamond). Each frame therefore is a projection in gyrophase (polar angle) and pitch angle (radial extent) for a single energy in the solar wind frame of reference. The plus signs toward the right represent the field direction, and the solar wind direction is indicated by asterisks. For each frame the color scales are individually normalized after subtraction of a background count rate, estimated from intervals when the spacecraft was not magnetically connected to the bow shock.

[18] The top frames of Figure 3 show the angular distribution taken during 2109:05–2109:17 UT and indicate field-aligned protons propagating sunward. The 18 and 14 keV channels show no protons, and examination of intermediate energy channels (not shown) indicate that the beams cut off above ~8 keV. At 2110:57–2111:09 UT and 2110:57–2111:41 UT the distributions clearly indicate that the lower-energy protons (E = 3.83 − 2.62 keV) are field aligned, whereas those at higher energies (E = 17.74 and 14.08 keV) are offset from the magnetic field axis and appear as arcs partially circumscribing the magnetic field. This is a signature of gyrating ions with limited gyrophase extent. Similar gyrating ion signatures appear for all energies at 2111:45 UT and later, simultaneous with the onset of magnetic fluctuations (Figure 1). For the low-energy channels the peak pitch angles remain rather small. During the same time interval, SC 3 measured nearly similar features (not shown here) while 0.08 R_E distant from SC 1.

4. Shock Geometry

[19] Various proposed shock reflection mechanisms [e.g., *Thomsen*, 1985, and references therein] predict that efficiencies and pitch angles of particles produced are strongly dependent on shock geometry (i.e., on θ_{Bn} and θ_{Vn}). Table 1 shows several bow shock-related parameters estimated from measurements obtained by SC 1 for four times prior to ULF onset and one time afterward. The third column of Table 1 shows the cone angle θ_{BV}, measuring the angle between the magnetic field direction and the solar wind

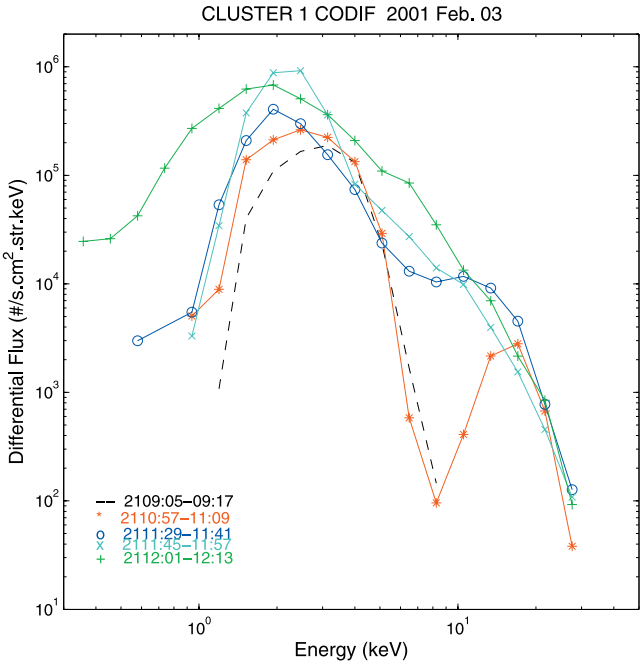

Figure 2. Energy spectra taken by Cluster 1 CODIF at successive time intervals.

direction. The fourth column lists θ_{Vn}, the angle between the solar wind velocity and the shock normal located where the field line threading the spacecraft intersects the bow shock. The fifth column provides θ_{Bn}. To compute these values, we have assumed that the field lines are straight and have used the statistical bow shock model of *Cairns et al.* [1995]. Convection was not included in these computations, but because of the geometry and proximity to the shock the affect is slight, <1°. Estimates of θ_{Vn} and θ_{Bn} are repeated for the statistical bow shock models from *Farris et al.* [1991] and *Slavin and Holzer* [1981]. These bow shock models are well described in the literature and are widely used.

[20] The gasdynamic bow shock models [*Farris et al.*, 1991; *Slavin and Holzer*, 1981] provide nearly identical values for both θ_{Bn} and θ_{Vn}. There is, however, a 2°–3° difference between θ_{Bn} values computed using these models and an MHD-based model [*Cairns et al.*, 1995]. Nearly identical results were obtained using observations from spacecrafts 3 (not shown) and 1.

[21] As indicated by Table 1, the interplanetary magnetic field (IMF) direction is quasi-steady in the time interval 2109:05–2111:41 UT (events a–d), and there is no evidence that the angle θ_{Bn} varied during this time. However, the beam parallel velocity noticeably decreases during this period. At ~2112 UT a small decrease of the IMF B_z component leads to changes in the shock geometry (Table 1), and it appears to be associated with the observed changes in the distribution functions.

[22] Table 1 includes parallel and perpendicular velocities associated with the lower-energy upstream proton component for each listed snapshot. These velocities, given in the solar wind frame of reference, were obtained using the reduced distribution functions $f(V_{\|})$ and $f(V_{\perp})$. Energy cutoffs have been applied to exclude the more energetic component seen in the energy spectrum shown in Figure 2.

5. Discussion

5.1. Boundary Separating Field-Aligned Beams From Gyrating Ions

[23] We have presented observations of a 1–30 keV upstream proton event characterized by a double-peaked energy spectrum. The event was observed nearly simultaneously by CIS instruments on board Cluster spacecrafts 1 and 3, which were separated by 500 km. We note that double-peaked spectrum profiles associated with upstream ions at these energies have not been reported previously. The primary peaks associated with field-aligned protons are frequently observed upstream of the quasi-perpendicular bow shock. The production of such ion beams results from either the reflection of a portion of the solar protons or leakage from the magnetosheath.

[24] In order to account for the simultaneous observation of the gyrating populations with the beams, we refer to the schematic in Figure 4, which presents three particle trajectories in the plasma frame. To the left of the figure, field lines are populated by field-aligned protons, while on the right they are populated by gyrating ions. Initially, the spacecraft is located to the left of the point labeled S, where it observes only field-aligned beams. When it is at S, it begins to sample the large-orbit gyrating 20 keV protons. Despite the 12-s CODIF integration periods that are comparable to a proton gyroperiod, the gyrophase ranges for the gyrating components are not spread out into a broad arc but instead are rather narrow. This is because the only gyrating particles reaching S originate from the field line shown on the right and can only arrive from one direction. This narrow gyrophase range is a signature expected when remotely sensing the sharp edge of a particle region [cf. *Meziane et al.*, 2003, Figure 4]. It is possible that there are also lower-energy gyrating protons centered on the same field line, but these would not be observed at S because of their smaller orbits. As θ_{Bn} decreases because of the rotation of the IMF, two features are predicted according to Figure 4: The detected gyrating ions should broaden in observed pitch angles as the locus of accessible guiding centers increases, and the detector should begin to detect gyrating ions with successively lower energies, if they exist. This corresponds to the picture presented in Figure 4, although the actual observations are more complex than this simple schematic would indicate.

[25] The detailed structure of the distributions in Figure 3 can be accounted for by noting the large $\delta B/B$, 40-s modulations of the magnetic field, which significantly affect the directions at which particles arrive at the detector within the three-spin integration periods. Phase space densities have been mapped according to 12-s magnetic field averages, and significant aliasing can be expected. For each of the three spacecraft spins during which distributions are accumulated, a given azimuthal angle has been sampled after rotation of the magnetic field, and in several cases this has led to an appearance of three distinct spots or arcs. Alternatively, we could say that corresponding to each spot or arc, there is a different one-spin-averaged magnetic field direction. The computed orientations for the magnetic field

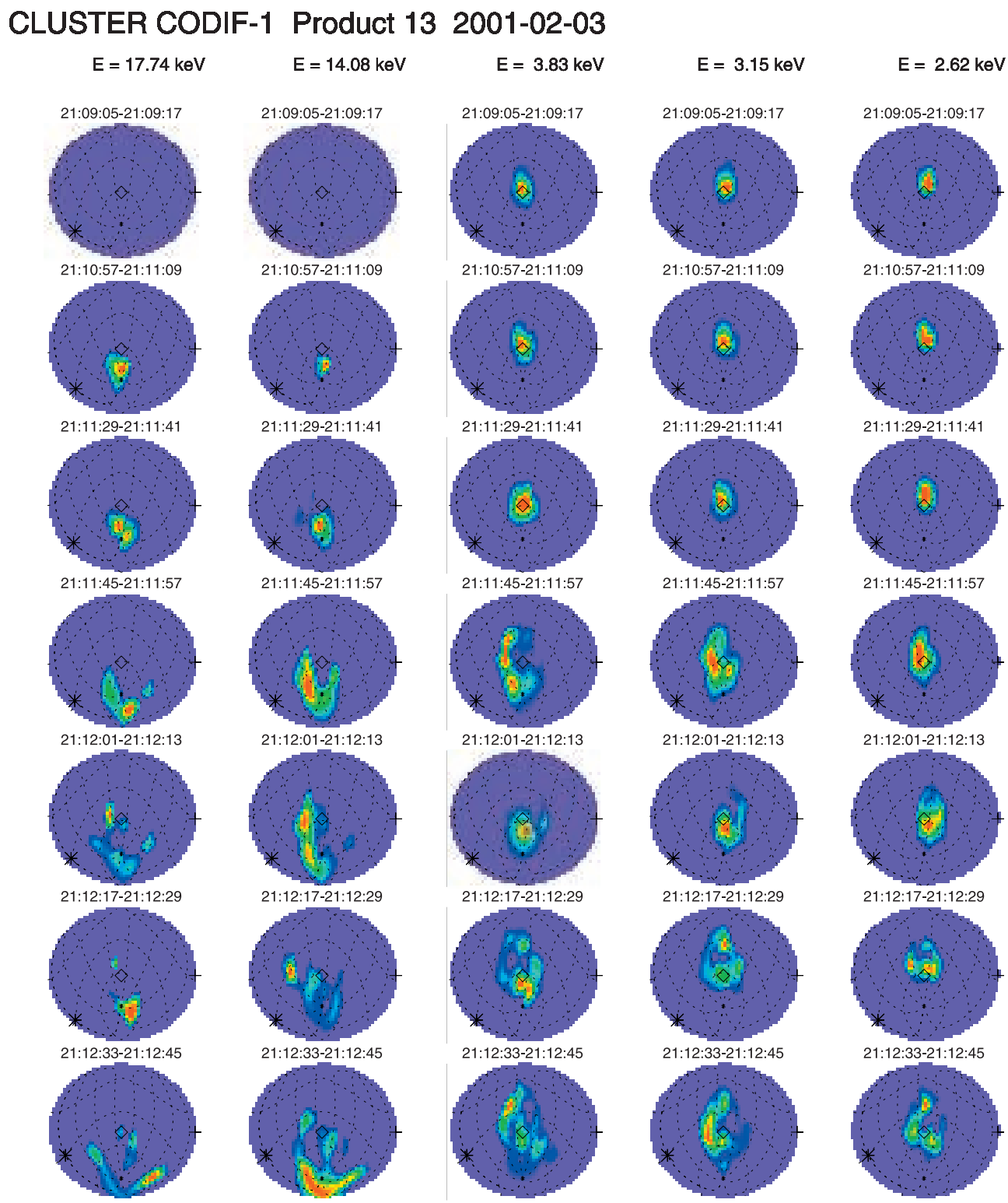

Figure 3. Successive three-dimensional distributions from Cluster 1 CODIF instrument for five energy channels. Details are in the text.

were seen to vary by 5°–60° between successive spin periods following the onset of the ULF waves.

[26] The coexisting field-aligned beams and 20 keV gyrating ions seen at 2110:57–2111:57 UT occurred before the ULF waves were observed at each spacecraft, but during their orbits the gyrating particles having gyroradii ~1200 km were likely to be sampling adjacent regions of physical space that were permeated with the large $\delta B/B$ fluctuations seen 1–2 min later. We note that the ~4 keV channel on spacecraft 3 at 2111:49–2112:01 UT appears to have a central PSD peak in addition to three PSD maxima within the surrounding arc. This appears to indicate a

Table 1. Cluster 1 Beam Velocities Computed in the Solar Wind of Reference and Shock Geometry Associated With the Ion Distributions

			Cairns et al. [1995]		*Farris et al.* [1991]		*Slavin and Holzer* [1981]			
Event	Time Interval, UT	θ_{BV}	θ_{Vn}	θ_{Bn}	θ_{Vn}	θ_{Bn}	θ_{Vn}	θ_{Bn}	$V_{\parallel}$, km s^{-1}	$V_{\perp}$, km s^{-1}
a	2109:05–2109:17	50	161	50	159	48	160	48	859 ± 18	76 ± 16
b	2110:57–2111:09	50	161	51	159	48	160	48	805 ± 24	110 ± 32
c	2111:29–2111:41	48	163	50	161	47	162	47	814 ± 25	93 ± 46
d	2111:45–2111:57	48	164	50	162	47	163	47	710 ± 30	141 ± 92
e	2112:01–2112:13	46	164	45	161	42	162	42	681 ± 30	281 ± 105

simultaneous measurement of two populations at the same energy.

[27] Given the relatively large number of studies of upstream ion distributions, we think it useful to address the absence of reports showing simultaneously observed energetic gyrating ions and field-aligned beams. Most likely, the observations presented here indicate distinct shock production regions for the two types of distributions and/or that if particles are modified after emerging from the shock, the conditions present upstream are similarly bounded. For a given shock crossing we would not expect to observe field-aligned beams simultaneously with gyrating ions if the regions were well separated or if the IMF rotated rapidly (i.e., enough during a distribution sampling time to shift the foreshock layer more than a gyroradius). It is no surprise, then, that simultaneous observations of field-aligned beams and gyrating ions are being reported first in Cluster observations, due to the high-time resolution ion measurements from CIS and the shock-skimming apogees of the orbits, which provide many samples from regions near the shock.

5.2. Comparison of P_{gc} With Other Observations and With Models

[28] We now examine the velocity of upstream protons propagating near the spatial limit (boundary) of the field-aligned beams observed here. It is conventional in the literature to express velocities as multiples of the solar wind speed, and we use this convention for an upstream ion's guiding center speed V_{gc} and parallel velocity $V_{\parallel}$ (measured in the solar wind frame). Using the multipliers $P_{\parallel}$ and P_{gc},

$$V_{gc} = P_{gc} V_{sw} \tag{1a}$$

$$V_{\parallel} = P_{\parallel} V_{sw}. \tag{1b}$$

Past results have been provided in terms of both P_{gc} and $P_{\parallel}$ so it is useful to be able to relate these two velocity ratios. Applying straightforward geometric arguments, *Meziane and d'Uston* [1998] showed that if θ_{BV} is known,

$$P_{gc} = \sqrt{1 + P_{\parallel}^2 - 2P_{\parallel}\cos\theta_{BV}}. \tag{2}$$

[29] Before comparing our observations to theory, we first note how our results compare with previous statistical studies. Referring to interval d in Table 1, the upstream ion beams seen along the boundary separating them from the gyrating ions have a parallel speed of $V_{\parallel}$ = 710 ± 30 km s^{-1}, leading to P_{gc} = 1.68 ± 0.08. *Bonifazi and Moreno* [1981a] determined a statistical average value of $\langle P_{gc} \rangle$ = 2.0 for reflected (field aligned) beams, and from the histogram in their Figure 4 we estimate a spread of ±0.5. It is useful to mention that P_{gc} is compared with P of *Bonifazi and Moreno* [1981a]. The result we have determined agrees better with the average speed ratios they found for intermediate and diffuse populations, namely, 1.75 and 1.18, respectively, both of which we estimate from the histogram variations of ±0.5. As mentioned in section 1, comparison of our result with the earlier statistical results is not straightforward because those results were compiled without discriminating between differing values of the cone angle θ_{BV}.

[30] Each of the models for foreshock ions discussed below has an explicit dependence on θ_{BV}, so we expect that our results for P_{gc} from a single shock crossing might be in disagreement with a statistical average over a wide range of shock geometries. However, the measured values of θ_{BV} ranging from 46° to 50° are very near the Parker spiral angle and could turn out to be well represented by a statistical study.

[31] The apparent existence of spatially distinct foreshock ion populations leads us to examine whether the field-

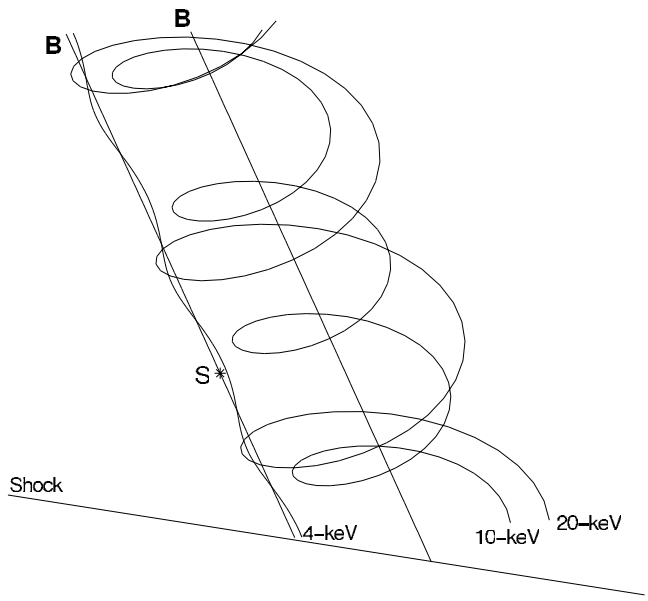

Figure 4. Simple sketch showing how a double-peaked spectrum is observed at the spacecraft location S, presenting orbits in the plasma frame.

aligned beam boundary reported here can be accounted for by foreshock ion source mechanisms often used in the literature. A well-known mechanism [*Sonnerup*, 1969] is based on the reflection of a portion of solar wind protons in a manner which can be viewed as quasi-adiabatic, that is, which to a degree preserves the particles' magnetic moments $\mu = V_\perp^2/B$ while conserving total energy in the deHoffman-Teller (dHT) frame. In general, this mechanism produces a high-speed proton beam with $P_{gc} \sim 2$. The factor $P_\parallel$ associated with the parallel velocity, expressed in the solar wind frame of reference, is given for thermal solar wind ions by

$$P_\parallel = -(1+\delta)\cos\theta_{Vn}/\cos\theta_{Bn}, \quad (3)$$

where $\delta = 1$ for the case of the magnetic moment being conserved exactly and $0 < \delta < 1$ otherwise.

[32] We note that only $\delta = 1$ produces field-aligned beams; if $\delta < 1$, the produced beam would have a pitch angle

$$\alpha = \arctan\sqrt{(1-\delta)/(1+\delta)}. \quad (4)$$

We then use θ_{Vn}, θ_{Bn}, and θ_{BV} values given in Table 1 to estimate the theoretical values for P_{gc}. In order to obtain the experimental value of $P_{gc} = 1.68$, it would be necessary to assume a value of $\delta \sim 0.5$, which leads to a pitch angle of $\alpha = 33°$ using equation (4). Since the field-aligned beams observed clearly had much smaller values of α, this reflection mechanism appears to be ruled out as a possible source.

[33] Another model used to account for field-aligned beams involves the leakage of magnetosheath particles. For this it is assumed that variations in the magnetic moment can be accounted for by their passage through the cross-shock electric potential [*Schwartz et al.*, 1983]. The maximal potential difference $\tilde{\phi}_{sh}$ across the shock is commonly estimated by equating it to a thermal solar wind proton's bulk kinetic energy

$$q\tilde{\phi}_{sh} = 1/2 m V_{sw}^2, \quad (5)$$

where q is the proton charge. Shock simulations at perpendicular geometries provide values of $\phi_{sh} \approx 0.6\ \tilde{\phi}_{sh}$ [*Sanderson and Uhrig*, 1978; *Leroy et al.*, 1982]. For the maximum potential drop described by equation (5), *Schwartz et al.* [1983] determined a parallel velocity ratio of

$$P_\parallel = -[1 + (1 - N/r)/\cos\theta_{Bn}]\cos\theta_{Vn}, \quad (6)$$

where N is the upstream to the downstream magnetic field ratio and r is the shock compression ratio. (This expression differs from that given by *Schwartz et al.* [1983] because here it is expressed in the solar wind frame of reference.)

[34] In order to estimate the N/r ratio, we apply the Rankine-Hugoniot continuity relations to the plasma and field conditions observed on the upstream side of the shock. The assumptions of a slab local geometry and coplanarity of the magnetic field **B**, flow velocity $\mathbf{V}_{sw}$, and shock normal **n** permit us to obtain their asymptotic counterparts and the plasma density for the downstream side.

[35] Using the solar wind parameters provided by the HIA instrument's low-geometry factor side, the magnetic field measurements obtained from the Magnetic Fields Investigation experiment, we have computed N/r ratios for shock geometries listed in Table 1; $\theta_{Bn} = 50°$ leads to $N/r = 0.80$, and $\theta_{Bn} = 47°$ yields $N/r = 0.78$. Substituting these values into equation (6), we obtain a leakage-predicted parallel velocity ratio of $P_\parallel \sim 1.22$ in both cases. This is substantially smaller than the $P_\parallel$ value measured at the field-aligned beam boundary. Recall that $P_\parallel$ was estimated via equation (6) assuming a maximum cross-shock potential drop of $\tilde{\phi}_{sh}$ (equation (5)), while numerical simulations of quasi-perpendicular shock structure indicate that the electrostatic potential is ~40% lower [*Leroy et al.*, 1982]. For $\phi_{sh} \approx 0.6\ \tilde{\phi}_{sh}$ the computed energy gain of particles escaping the magnetosheath is correspondingly lower, resulting in worse agreement with the observations. We conclude therefore that the particle leakage from the magnetosheath is not a satisfactory mechanism for the observed field-aligned proton boundary.

[36] Another source mechanism for backstreaming ions was reported by *Tanaka et al.* [1983]. In this model, field-aligned beams emerge from the magnetosheath in quasi-perpendicular bow shock regions. In the process simulated, highly anistropic dowsntream particle distributions excite electromagnetic ion cyclotron instabilities, which in turn scatter the ions. Those acquiring high parallel velocities can escape upstream. For typical solar wind conditions and IMF directions ($\theta_{BV} \sim 45°$), as was nearly the case for the event we report here, Tanaka et al.'s model predicts P_{gc} values ~2, smaller than those obtained for the reflection mechanism but still significantly higher than those measured for the field-aligned proton boundary.

[37] In summary, we have reviewed three known source models for upstream ions and have found that none is consistent with the observed beam velocities. We stress that the failure of the quasi-adiabatic [*Sonnerup*, 1969] or the magnetosheath leakage mechanisms to explain the field-aligned beam velocity has been reported in previous studies. *Thomsen et al.* [1983b] showed that μ-conserving reflection is not satisfied for a score of field-aligned beams initially reported by *Paschmann et al.* [1980]. Nor can the observed beam velocities be accounted for by assuming μ-conserving leakage [*Thomsen et al.*, 1983b]. One way of obtaining better agreement would be to adjust the parameter δ in equation (3). This, however, conflicts with the observed field-aligned character of the beams. A minimum value of $\delta = 0.6$ has been reported in the literature [*Bonifazi et al.*, 1983]. This value leads to a pitch angle ~27° (according to equation (4)), too high to match our observations. If we consider, for example, the proton beam observed at 2109:05–2109:17 UT (interval a), the measured parallel velocity is in good agreement with the reflection mechanism (equation (3)) if $\delta \sim 0.78$. This would lead to $\alpha = 20°$, significantly higher than the pitch angles observed. We should also mention that the energy conservation assumed in this relationship is probably violated for most field-aligned beams (Wilber et al., submitted manuscript, 2003).

[38] There is some uncertainty in the estimation of θ_{Bn}, but the very high agreement (to within ±2°) using the three different statistical bow shock models suggests that these estimates are reasonable. Strongly dynamic condi-

tions, such as those seen after 2112:30 UT, would invalidate the assumed simple geometric surface, but we are considering earlier intervals that were observed to be steady. A few degrees of error in this parameter would not affect the general conclusions of the previous comparisons between the observed upstream ions and production models.

[39] On the other hand, we note that the statistical bow shock models used here are time-independent for fixed interplanetary conditions. These models are probably satisfactory in a time-averaged sense. Many supercritical collisionless magnetosonic shock simulations indicate that for timescales comparable to the downstream gyroperiod the shock is probably nonstationary for a relatively large θ_{Bn} range. For quasi-perpendicular geometries the nonstationarity results from a shock self-re-formation caused by the accumulation of reflected ions in the shock front [*Lembege and Savoini*, 1992]. More commonly, at lower ranges of θ_{Bn} this shock re-formation occurs mainly because of large magnetic structures, always present in quasi-parallel shock regions, convecting into the shock and destabilizing it [*Burgess*, 1989; *Thomas et al.*, 1990]. The shock variability would certainly affect the ion acceleration conditions, while the remotely determined estimation of the shock geometry remains unchanged because of the stability of the solar wind and IMF upstream conditions. This may lead to inaccuracies in the predicted parallel velocities.

5.3. The Compressional Wave Boundary

[40] As described in the introduction, the MHD-like waves excited by field-aligned beams are believed to be responsible for the pitch angle scattering of post foreshock ions into intermediate and diffuse distributions [*Lee and Skadron*, 1985]. Because of their finite growth rates and moderate phase velocities the outward propagating waves are convected downstream from their initiation points along the outer edge of the ion foreshock boundary. When they are observed in association with intermediate, diffuse, or gyrating ions, their amplitudes are significant. The onset of these well-developed ULF waves appears to be consistent with the ULF foreshock boundary previously reported by *Greenstadt and Baum* [1986]. The observations presented here also match previous studies, which showed no ULF waves in regions containing field-aligned beams.

[41] *Skadron et al.* [1988] theoretically investigated the spatial and temporal evolution of the ULF waves and determined the location of a compressional wave boundary. This boundary was defined by points where the wave amplitude is just above the ambient solar wind magnetic field variation level. The observed boundary, they noted, would be farther downstream where the amplitudes are larger.

[42] We should expect, then, that the backstreaming ions present at the wave compressional boundary are still propagating nearly along the ambient magnetic field; the pitch angle scattering is still weak given the low amplitude at this growth stage, even though the effects of the waves on the particles could be noticeable. In the study by *Skadron et al.* [1988] the evolution of the particle distribution has not been quantitatively addressed in detail; we should, however, expect that the ions are still nearly propagating along the ambient IMF direction.

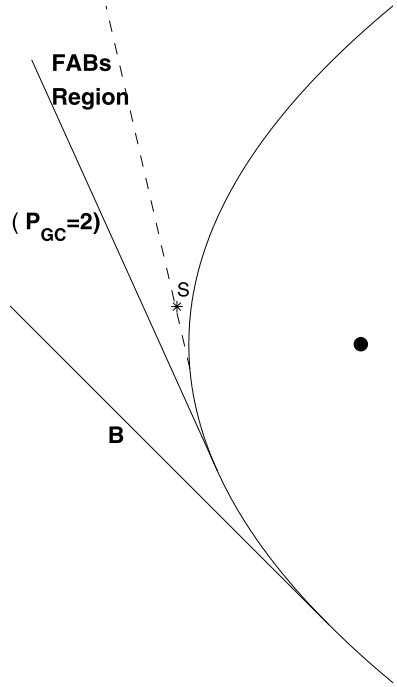

Figure 5. Sketch showing the location of the outer boundary for foreshock field-aligned beam with the cone angle $\theta_{BV} = 45°$.

[43] One way to see whether their wave compressional boundary is consistent with the field-aligned boundary reported here is to compare the two slopes. *Skadron et al.* [1988] showed that for typical solar wind conditions and a cone angle $\theta_{BV} = 45°$ the compressional wave boundary makes an angle of 78° with respect to the x_{GSE} axis. Applying geometric arguments, *Meziane and d'Uston* [1998] showed that the direction of the guiding center of a proton having a parallel velocity $V_{\|} = P_{\|} V_{sw}$ (in the solar wind frame of reference) makes with respect to x_{GSE} an angle ζ given by

$$\tan\zeta = \frac{P_{\|}\sin\theta_{BV}}{P_{\|}\cos\theta_{BV} - 1}. \quad (7)$$

Using the observables for event d presented in Table 1, we find $\zeta = 77° \pm 3°$, in agreement with the predicted ULF boundary of *Skadron et al.* [1988].

[44] Figure 5 is a sketch of the convection limits for field-aligned beams during this interval. The dashed line corresponds to $P_{gc} = 1.68$ discussed in section 5.2 and associated with the last observed field-aligned beam. The solid line corresponds to $P_{gc} = 2$, which is the average beam speed based on the statistical study of *Bonifazi and Moreno* [1981a]. This value is conventionally taken as the ion foreshock boundary, but the outer spatial limit for field-aligned beams for a given cone angle remains to be investigated. The shock shape and convection boundaries are based on projections of the beam to the model bow shock [*Cairns et al.*, 1995].

[45] Also, the distance along the x_{GSE} axis separating the field-aligned boundary from the conventional ion foreshock boundary at $P_{gc} = 2$ can be computed. We found that this

distance, estimated at the spacecraft location, is $D_x \sim 5\ R_E$. Previous observations based on ISEE data [*Bavassano-Cattaneo et al.*, 1983] indicate that the intermediate region between the field-aligned beam and the diffuse ion population is located at $D_x \sim 5\ R_E$, in good agreement with the findings of the present work. Figure 5 shows the projected spacecraft position S on the boundary reported here.

[46] Finally, another interesting aspect of the boundary concerns its position with respect to the shock surface, best studied with θ_{Bn}. Table 1 indicates that the boundary intersects the bow shock at $\theta_{Bn} = 50°$, the lower bound of the quasi-perpendicular shock determined by [*Skadron et al.*, 1988]. *Le and Russell* [1992] analyzed 373 bow shock crossings and found no IMF fluctuations for $\theta_{Bn} > 50°$, consistent with our results.

5.4. Origin of Gyrating Ions

[47] We now examine the guiding center velocity associated with the gyrating ions observed just downstream of the field-aligned boundary. Typically, our observations show that only the high-energy part of the gyrating ion distributions appears simultaneously with the field-aligned beam. While the field-aligned beams are still observed, the spectral peak of the gyrating ion population is not observed (Figure 2; only the high-energy part is observed because of the larger gyroradii of these particles).

[48] At 2112:01–2112:13 UT (Table 1, event e) the guiding center velocity was $P_{gc} = 1.52 \pm 0.08$ (Figure 2). This is the first interval during which spacecraft 1 was able to observe the lower-energy extent of the gyrating component's spectrum (peaked near 1.5 keV), and this value of P_{gc} may be taken as the upstream limit for this population. Gyrating ions >10 keV were detected during the previous four CIS integrations, and these had similar pitch angle ranges ($22° \pm 8°$) for the peak phase space densities. The arguments provided in section 5.1 would indicate that these were from essentially the same population, remotely sensed, obviating the need to speculate on the guiding center speeds of gyrating ions closer to the field-aligned beams.

[49] As described in section 1, *Meziane and d'Uston* [1998] investigated foreshock ions using a unidirectional detector that would observe field-aligned beams only in rare configurations of the IMF and the spacecraft location. Nearly always, they were observing intermediate, diffuse, and possibly gyrating ions. It is notable that their results show that when such an ion foreshock boundary is found for $\theta_{BV} = 45°$, the ion guiding center speed is $P_{gc} = 1.11 \pm 0.04$, significantly smaller than our present results. The most likely explanation for this difference is that the boundary found by *Meziane and d'Uston* [1998] using a unidirectional instrument was associated with diffuse populations rather than gyrating ions. Another study carried out by *Le and Russell* [1992] identified ULF foreshock boundary crossings. For $\theta_{BV} = 45°$ the authors found that the streaming speed associated with the ULF foreshock boundary was $P_{gc} = 1.5$, in remarkable agreement with the streaming speeds presented here for the gyrating foreshock ion boundary.

[50] One hypothesis based on this mechanism, first reported by *Gosling et al.* [1982], involves the specular reflection of a portion of the incoming solar wind ions. For this, the normal component of incident particle velocity is reversed in the dHT frame, while the tangential component remains unchanged. Using the values for event e of Table 1, we find that the measured values for the parallel velocity component (681 ± 30 km s^{-1}) is substantially higher than the one predicted for the case of specular reflection (228 km s^{-1}). The failure to find agreement between this model and our observations could be expected, as the analysis of orbital motions has shown that specularly reflected ions may only escape upstream if produced at $\theta_{Bn} \leq 40°$ [*Schwartz et al.*, 1983].

[51] Gyrating ion distributions might also be explained by a kinematic description that has magnetosheath particles transmitted across the shock, initially directed along the shock normal **n** [*Schwartz et al.*, 1983]. The particle energy gain is mostly due to the cross-shock potential jump. To date, comparisons of this mechanism with observations have shown poor agreement [*Thomsen et al.*, 1983b]. In the present case, a quantitative comparison is also possible. For a maximum electrostatic potential jump, $\phi_{sh} = \tilde{\phi}_{sh}$, the minimum value of $P_{\|}$ for escaping ions is given by

$$P_{\|} = -(1 - N/r)\cos\theta_{Vn}[\cos\theta_{Bn} + 1/\cos\theta_{Bn}]. \qquad (8)$$

[52] As in section 5.2, we estimate the N/r ratio using θ_{Bn} and θ_{Vn} values given in Table 1 as well as the plasma and the IMF data. We find that $N/r = 0.72$ and 0.71 for $\theta_{Bn} = 43°$ and $\theta_{Bn} = 42°$, respectively. The parallel velocity 183 km s^{-1} obtained is substantially smaller than that observed. As before, a weaker cross-shock potential ϕ_{sh} would increase the disagreement.

[53] Finally, a comparison of our results with numerical simulations is appropriate. Numerous simulations of different types of shock-associated energetic particle have been reported [*Burgess*, 1987; *Leroy et al.*, 1981]. Regardless of the nature of these numerical simulations, 1-D or 2-D, hybrid and full particle, they all show that supercritical collisionless shocks cause the emission of backstreaming particles for a large range of θ_{Bn}. Interestingly, a hybrid numerical simulation of a 1-D oblique shock ($\theta_{Bn} \sim 45°$) [*Leroy and Winske*, 1983], corresponding to the geometry of interest here, shows that a significant fraction of incoming particles is reflected at the shock, which remains rather stationary. (This 1-D simulation only allowed for coplanarity and may have suppressed re-formation processes.) The backsteaming particles have a large span of pitch angles, and the resulting distributions can exhibit characteristics more like gyrating ions than field-aligned beams. The parallel and the perpendicular velocities, in the solar wind frame of reference, typically have speeds of 2.5 and 1 times the solar wind speed, inconsistent with the adiabatic reflection hypothesis and the specular reflection mechanism. There is a small fraction of the backstreaming particles that does agree with the prediction of the specular reflection. We should stress that the velocities obtained from the numerical simulations agree reasonably well with the observed velocity associated with the gyrating ions (event f).

[54] The disagreement between the observed guiding center speeds and those predicted for specularly reflected ions, or ions leaking from the magnetosheath across a shock potential θ_{sh}, suggests that these gyrating ions may originate

as beams that are modified en route from the shock. Field-aligned beams can be disrupted through the electromagnetic ion beam instability [*Gary et al.*, 1981], but the predicted growth rates, and the presence of stable beams on adjacent field lines, make this implausible as a sole mechanism for the gyrating ions seen at the boundary. The ULF waves seen starting with this boundary may indeed arise from the electromagnetic ion beam instability [*Mazelle et al.*, 2000] and then convect into more quasi-parallel regions where they modify particles emerging from the shock. *Winske and Leroy* [1984] showed how these ULF waves could pitch angle scatter beams to produce diffuse distributions. Recently, *Meziane et al.* [2001] showed observations indicating an association of gyrating ions with ULF waves, similar to the case presented here, and those may have resulted from wave trapping during the early stages of wave growth [*Hoshino and Terasawa*, 1985]. Such a test for wave trapping is beyond the scope of this study.

6. Conclusion

[55] We have reported on observations of briefly overlapping field-aligned and gyrating ion populations, in a region upstream of the Earth's oblique bow shock. We have interpreted these to indicate a very sharp transition between the two populations, spanning no more than a gyroradius. The observations occurred during typical solar wind conditions and with an IMF cone angle at the Parker spiral value of $\theta_{BV} \sim 45°$. The downstream limit of the field-aligned beams intersected the bow shock where $\theta_{Bn} \sim 50°$ and made an angle of $\sim 77°$ with respect to the Sun-Earth direction. These characteristics are in excellent agreement with the wave compressional boundary predicted by *Skadron et al.* [1988]. The protons propagating along this boundary have guiding center speeds inconsistent with the shock mechanisms proposed to date to account for the production of field-aligned beams. From Figure 2 we can see the modest decreases in proton beam speeds and a weak broadening in temperature between 2109:05 and 2111:41 UT (events a–d). While the computed values for θ_{Bn} during this interval did not change, the $\pm 2°$ uncertainty may have marked a small change in shock geometry that would account for these variations. Alternatively, the presence of very small amplitude ULF variations toward the end may have had some role in the temperature broadening observed.

[56] The gyrating ions observed just downstream of the boundary were similarly observed to have guiding center speeds inconsistent with proposed production mechanisms. The guiding center, however, agrees well with previous observations reported by *Le and Russell* [1992] and reasonably well with hybrid simulations. The onset of large-amplitude ULF waves at the boundary strongly suggests that they have a role in the form of the observed gyrating ion distributions. The failure of proposed production mechanisms to account for the observed guiding center speeds indicates a need for additional theoretical work.

[57] **Acknowledgments.** K.M. thanks I. H. Cairns for providing the code for the bow shock model and E. Penou for his assistance. Work at the University of New Brunswick is supported by the Canadian Natural Science and Engineering Council. Work at the University of California, Berkeley is supported by NASA grant NAG5-10131. Part of the work of K.M. has been supported by funding from CNRS. K.M and C.M. thank ISSI for its support.

[58] Shadia Rifai Habbal thanks Giovanni Moreno and Dan Winske for their assistance in evaluating this paper.

References

Balogh, A., et al. (2001), The Cluster magnetic field investigation: Overview of in-flight performance and initial results, *Ann. Geophys.*, *19*, 1207–1217.

Bavassano-Cattaneo, M. B., C. Bonifazi, M. Dobrowolny, M. Moreno, and C. T. Russell (1983), Distribution of MHD wave activity in the foreshock region and properties of backstreaming protons, *J. Geophys. Res.*, *88*, 9280–9286.

Bonifazi, C., and G. Moreno (1981a), Reflected and diffuse ions backstreaming from the Earth's bow shock: 1. Basic properties, *J. Geophys. Res.*, *86*, 4381–4396.

Bonifazi, C., and G. Moreno (1981b), Reflected and diffuse ions backstreaming from the Earth's bow shock: 2. Origin, *J. Geophys. Res.*, *86*, 4397–4404.

Bonifazi, C., G. Moreno, and C. T. Russell (1983), Reflection of the solar wind ions at the Earth's bow shock: Energization, *J. Geophys. Res.*, *88*, 7853–7859.

Burgess, D. (1987), Simulations of backstreaming ion beams formed at oblique shock by direct reflection, *Ann. Geophys., Ser. A*, *5*, 133–146.

Burgess, D. (1989), Cyclic behavior at quasi-parallel collisionless shocks, *Geophys. Res. Lett.*, *16*, 345–348.

Cairns, I. H., D. H. Fairfield, R. R. Anderson, V. E. H. Carlton, K. I. Paularena, and A. J. Lazarus (1995), Unusual locations of Earth's bow shock on September 24–25, 1987: Mach number effects, *J. Geophys. Res.*, *100*, 47–62.

Edmiston, J. P., C. F. Kennel, and D. Eichler (1982), Escape of heated ions upstream of quasi-parallel shocks, *Geophys. Res. Lett.*, *9*, 531–534.

Farris, M. H., S. M. Petrinec, and C. T. Russell (1991), The thickness of the magnetosheath: Constraints on the polytropic index, *Geophys. Res. Lett.*, *18*, 1821–1824.

Fuselier, S. A., M. F. Thomsen, J. T. Gosling, S. J. Bame, and C. T. Russell (1986), Gyrating and intermediate ion distributions upstream from the Earth's bow shock, *J. Geophys. Res.*, *91*, 91–99.

Gary, S. P., J. T. Gosling, and D. W. Forslund (1981), The electromagnetic ion beam instability upstream of the Earth's bow shock, *J. Geophys. Res.*, *86*, 6691–6696.

Giacolone, J., J. R. Jokipii, and J. Kóta (1994), Ion injection and acceleration at quasi-perpendicular shocks, *J. Geophys. Res.*, *99*, 19,351–19,358.

Gosling, J. T., J. R. Asbridge, S. J. Bame, G. Paschmann, and N. Sckopke (1978), Observations of two distinct population of bow shock ions in the upstream solar wind, *Geophys. Res. Lett.*, *5*, 957–960.

Gosling, J. T., M. F. Thomsen, S. J. Bame, W. C. Feldman, G. Paschmann, and N. Sckopke (1982), Evidence for speculary reflected ions upstream from the quasi-parallel bow shock, *Geophys. Res. Lett.*, *9*, 1333–1336.

Greenstadt, E. W., and L. W. Baum (1986), Earth's compressional foreshock boundary revisited: Observations by the ISEE 1 magnetometer, *J. Geophys. Res.*, *91*, 9001–9006.

Gurgiolo, C., G. K. Parks, B. H. Mauk, C. S. Lin, K. A. Anderson, R. P. Lin, and H. Rème (1981), Non-$\mathbf{E} \times \mathbf{B}$ ordered ion beams upstream of the Earth's bow shock, *J. Geophys. Res.*, *86*, 4415–4424.

Gurgiolo, C., G. K. Parks, and B. H. Mauk (1983), Upstream gyrophase bunched ions: A mechanism for creation at bow shock and the growth of velocity space structure through gyrophase mixing, *J. Geophys. Res.*, *88*, 9093–9100.

Hoshino, M., and T. Terasawa (1985), Numerical study of the upstream waves excitation mechanism: 1. Nonlinear phase bunching of beam ions, *J. Geophys. Res.*, *90*, 57–64.

Le, G., and C. T. Russell (1992), A study of ULF wave foreshock morphology. I. ULF foreshock boundary, *Planet. Space Sci.*, *40*, 1203–1213.

Lee, M. A., and G. Skadron (1985), A simple model for formation of "reflected," "intermediate," and "diffuse" ion distributions upstream of the Earth's bow shock, *J. Geophys. Res.*, *90*, 39–45.

Lembege, B., and P. Savoini (1992), Nonstationarity of a two-dimensional quasi-perpendicular supercritical collisionless shock by self-reformation, *Phys. Fluids B*, *4*, 3533–3548.

Leroy, M. M., and D. Winske (1983), Backstreaming ion from oblique Earth bow shocks, *Ann. Geophys.*, *1*, 527–536.

Leroy, M. M., C. C. Goodrich, D. Winske, C. S. Wu, and K. Papadopoulos (1981), Simulation of a perpendicular bow shock, *Geophys. Res. Lett.*, *8*, 1269–1272.

Leroy, M. M., D. Winske, C. C. Goodrich, C. S. Wu, and K. Papadopoulos (1982), The structure of perpendicular bow shocks, *J. Geophys. Res.*, *87*, 5081–5094.

Lin, R. P., C.-I. Meng, and K. A. Anderson (1974), 30- to 100-keV protons upstream from the Earth's bow shock, *J. Geophys. Res.*, *79*, 489–498.

Mailing, D. H. (1992), *Coordinate Systems and Map Projections*, 2nd ed., Pergamon, New York.

Mazelle, C., D. LeQuéau, and K. Meziane (2000), Nonlinear wave-particle interaction upstream from the Earth's bow shock, *Nonlinear Processes Geophys.*, *7*, 185–190.

Mazelle, C., et al. (2003), Production of gyrating ions from nonlinear wave-particle interaction upstream from the Earth's bow shock: A case study from Cluster-CIS, *Planet. Space Sci.*, 785–795.

Meziane, K., and C. d'Uston (1998), A statistical study of the upstream intermediate ion boundary in the Earth's foreshock, *Ann. Geophys.*, *16*, 125–133.

Meziane, K., C. Mazelle, R. P. Lin, D. LeQuéau, D. E. Larson, G. K. Parks, and R. P. Lepping (2001), Three-dimensional observations of gyrating ion distributions far upstream from the Earth's bow shock and their association with low-frequency waves, *J. Geophys. Res.*, *106*, 5731–5742.

Meziane, K., M. Wilber, R. P. Lin, and G. K. Parks (2003), Gyrophase-restricted 100 keV–2 MeV ion beams near the foreshock boundary, *Geophys. Res. Lett.*, *30*(20), 2049, doi:10.1029/2003GL017592.

Meziane, K., et al. (2004), Bow shock specularly reflected ions in the presence of low frequency electromagnetic waves: A case study, *Ann. Geophys.*, in press.

Möbius, E., et al. (2001), Observations of the spatial and temporal structure of field-aligned beam and gyrating ring distributions at the quasi-perpendicular bow shock with Cluster CIS, *Ann. Geophys.*, *19*, 1411–1420.

Paschmann, G., N. Sckopke, J. R. Asbridge, S. J. Bame, and J. T. Gosling (1980), Energization of solar wind ions by reflection from the Earth's bow shock, *J. Geophys. Res.*, *85*, 4689–4693.

Paschmann, G., N. Sckopke, I. Papamastorakis, J. R. Asbridge, S. J. Bame, and J. T. Gosling (1981), Characteristics of reflected and diffuse ions upstream from the Earth's bow shock, *J. Geophys. Res.*, *86*, 4355–4364.

Rème, H., et al. (2001), First multispacecraft ion measurements in and near the Earth's magnetosphere with identical Cluster ion spectrometry (CIS) experiment, *Ann. Geophys.*, *19*, 1303–1354.

Sanderson, J. J., and R. A. Uhrig Jr. (1978), Extended Rankine-Hugoniot relations for collisionless shocks, *J. Geophys. Res.*, *83*, 1395–1400.

Schwartz, S. J., M. F. Thomsen, and J. T. Gosling (1983), Ions upstream of the Earth's bow shock: A theoretical comparison of alternative source populations, *J. Geophys. Res.*, *88*, 2039–2047.

Skadron, G., R. T. Holdaway, and M. A. Lee (1988), Formation of the wave compressional boundary in the Earth's foreshock, *J. Geophys. Res.*, *93*, 11,354–11,362.

Slavin, J. H., and R. E. Holzer (1981), Solar wind flow about terrestrial planets: 1. Modeling bow shock position and shape, *J. Geophys. Res.*, *86*, 11,401–11,418.

Sonnerup, B. U. O. (1969), Acceleration of particles reflected at a shock front, *J. Geophys. Res.*, *74*, 1301–1304.

Tanaka, M., C. C. Goodrich, D. Winske, and K. Papadopoulos (1983), A source of the backstreaming ion beams in the foreshock region, *J. Geophys. Res.*, *88*, 3046–3054.

Thomas, V. A., D. Winske, and N. Omidi (1990), Re-forming supercritical quai-parallel shocks: 1. One- and two-dimensional simulations, *J. Geophys. Res.*, *95*, 18,809–18,819.

Thomsen, M. F. (1985), Upstream suprathermal ions, in *Collisionless Shocks in the Heliosphere: A Tutorial Review*, *Geophys. Monogr. Ser.*, vol. 34, edited by R. G. Stone and B. T. Tsurutani, pp. 253–270, AGU, Washington, D. C.

Thomsen, M. F., J. T. Gosling, S. J. Bame, W. C. Feldman, G. Paschmann, and N. Sckopke (1983a), Field-aligned ion beams upstream of the Earth's bow shock: Evidence for a magnetosheath source, *Geophys. Res. Lett.*, *10*, 1207–1210.

Thomsen, M. F., S. J. Schwartz, and J. T. Gosling (1983b), Observational evidence on the origin of ions upstream of the Earth's bow shock, *J. Geophys. Res.*, *88*, 7843–7852.

Winske, D., and M. M. Leroy (1984), Diffuse ions produced by electromagnetic ion beam instability, *J. Geophys. Res.*, *89*, 2673–2688.

M. B. Bavassano-Cattaneo, CNR-IFSI, Area di Ricerca di Toz Vergata, Via del Fosso del Cavaliere, Roma, I-00133, Italy. (bice@ifsi.rm.cnr.it)

J. M. Bosqued, I. Dandouras, C. Mazelle, H. Rème, and J. A. Sauvaud, CESR, 9 Ave. du Colonel Roche, Toulouse, F-31028, France. (bosqued@cesr.fr; dandouras@cesr.fr; mazelle@cesr.fr; reme@cesr.fr; sauvaud@cesr.fr)

A. M. Hamza and K. Meziane, Physics Department, University of New Brunswick, Fredericton, New Brunswick, Canada E3B 5A3. (ahamza@unb.ca; karim@unb.ca)

B. Klecker, Max-Planck Institut für Extraterrestrische Physik, Garching, D-85741, Germany. (bek@mpe.mpg.de)

A. Korth, Max-Planck Institut für Aeronomie, Katlenburg-Lindau, D-37191, Germany. (korthsprotte@mpae.gwdg.de)

H. Kucharek, Department of Physics and Institute for the Study of Earth, Oceans and Space, University of New Hampshire, Durham, NH 03824, USA. (kucharek@atlas.sr.unh.edu)

D. LeQuéau, Observatoire Midi-Pyrénées, 14 Ave. Edouard Belin, Toulouse, F-31400, France. (dominique.lequeau@obs-mip.fr)

E. A. Lucek, Blackett Laboratory, Imperial College London, London SW7 2BW, UK. (e.lucek@imperial.ac.uk)

R. N. Lundin, Swedish Institute for Space Physics, Kiruna, SE-98128, Sweden. (rickard.lundin@irf.se)

M. McCarthy, Earth and Space Sciences, University of Washington, Seattle, WA 98195, USA. (mccarthy@u.washington.edu)

G. K. Parks and M. Wilber, Space Sciences Laboratory, University of California, Berkeley, CA 94720, USA. (parks@ssl.berkeley.edu; wilber@ssl.berkeley.edu)